Artificial intelligence (AI) driven 3D point scanner for monitoring soil plug hazards during the installation of suction caisson foundations.

B. Williams, S. Suryasentana & M. Perry
University of Strathclyde, Department of Engineering, Glasgow, Scotland

K. Donaldson
University of Edinburgh, Department of Engineering, Edinburgh, Scotland

ABSTRACT: Soil plug hazards pose a significant risk to the successful installation of suction caisson foundations but are currently inadequately monitored using only a single beam echosounder. To address this issue, a new artificial intelligence (AI) driven three-dimensional (3D) point scanner is proposed for monitoring soil plug hazards. The proposed scanner is controlled using a Bayesian Optimisation (BO) algorithm, which automatically adapts its data acquisition path in real-time based on previously acquired measurements. Preliminary laboratory tests were conducted to assess the effectiveness of the proposed scanner. The results showed that the proposed scanner can accurately estimate 3D surfaces with fewer measurement points than a comparable scanner using the conventional scanning method, typically used in existing 3D point scanners. As the proposed scanner can estimate the state of the entire surface in much shorter time than existing sensors, it potentially offers a more effective method to monitor soil plug hazards.

1 **Introduction**

Suction caissons are a type of offshore foundation that serve as an alternative to the commonly used monopile foundations. They resemble upturned buckets (Byrne et al., 2002) and have a unique suction-aided installation procedure. First, the caisson is left to penetrate the seafloor under its own weight to form a seal. Once the seal is formed, a pump is used to remove water from inside the caisson, creating a pressure difference between the inside of the caisson and the ambient pressure. This pressure difference drives the caisson downward into the seabed (OWA, 2019).

Suction caissons offer several advantages over monopiles. They can be cheaper to install since there is no need for pile-driving equipment and they can be installed faster without requiring specially modified vessels. In addition, their installation produces less noise, which makes them less harmful to marine life. Furthermore, when it comes to decommissioning, they can be easily removed by reversing the pumping process, making them a more environmentally friendly option (He et al., 2022). However, caissons cannot be installed in areas with coarse materials or large boulders. Large boulders prevent caisson penetration, and coarse materials prevent an adequate seal from forming, stopping any pressure build-up.

Despite the potential advantages of suction caissons, installing suction caissons can be challenging due to potential hazards. Soil plug hazards, such as soil heave and soil plug uplift, are of great concern, as they can significantly impact the installation process. Soil plug heave occurs when the soil plug (i.e., the soil volume inside the caisson) rises upwards due to suction pressure and soil being displaced by the caisson skirt moves inside the caisson (Andersen and Jostad, 2002). On the other hand, soil plug uplift happens when the soil plug detaches itself from the seabed due to high suction pressures and variations in soil conditions (Ragni et al., 2022). Soil plug uplift has been shown to occur in layered soils, particularly when clay overlays sand (Ragni et al., 2022).

Skirt tip injection, a process where water is pumped at high pressure around the tip of the caisson, has been used to reduce the soil resistance to penetration (Aas et al., 2009). This allows the required suction pressure to remain much lower than the limit governed by the soil bearing capacity, thus reducing the risk of the soil plug hazards. Effective risk management and mitigation of soil plug hazards require early detection of these hazards during caisson installation. Therefore, this paper focuses on developing a new monitoring solution to detect soil plug hazards during caisson installation.

2 **Methodology**

2.1 *Current Practice*

Current practice for monitoring soil plug hazards involves placing a single beam echosounder through the hole on the caisson lid where the pump is mounted

(Sparrevik et al., 2015). However, this practice provides limited feedback on the overall state of the soil plug, since the single beam echosounder can only observe the area directly below itself. If the soil plug were to rise in any other location not illuminated by the echosounder, it would go undetected and potentially cause issues during installation. Therefore, it is necessary to develop a device that can observe multiple locations on the surface of the soil plug to improve the monitoring process.

Using a three-dimensional (3D) scanner is potentially an effective option to monitor soil plug hazards, as it can observe the entire surface of the soil plug. Examples of 3D scanners that could be used include multibeam echosounders (Teledyne BV5000, Coda Octopus Echoscope), 3D mechanical scanning sonar (Kongsberg DAS, Echologger DASS710), underwater lidar (3DatDepth SL4), and underwater laser line scanners (Voyis insight nano, micro, and pro). However, there are challenges associated with these devices. They can be very expensive, costing tens of thousands of pounds, which could limit their adoption in the industry. Some devices are also too large to fit through the hole on the caisson lid. Multibeam ultrasound devices may experience interference in a tight space, resulting in inaccurate readings (Cain and Leonessa, 2012). There are concerns that laser devices may not have the required range or be significantly affected by water turbidity (Zhang et al., 2017). However, the greatest challenge is that all existing underwater 3D scanners are considered too slow to effectively monitor the dynamic state of the soil plug during installation. Conventional 3D scanning methods used in commercial devices can take up to 30 minutes to complete a full hemispherical scan. Given the expected penetration speed of the caisson during installation, the state of the full soil plug surface will ideally need to be estimated every minute for effective detection of soil plug hazards.

The conventional scanning method is slow because it involves taking many thousands of measurement points per scan, even though many of these points might be redundant and might not provide much new information. To speed up the process, it may be possible to reduce the number of measurements taken per scan and predict the entire soil plug surface from these measurements. However, an effective method for selecting the optimal and most informative locations to take these measurements is necessary to ensure that the accuracy of the predicted soil plug surface is not compromised.

2.2 *Gaussian Process Regression*

Gaussian process (GP) models are a powerful tool for nonlinear regression (Suryasentana and Sheil, 2023). In this study, they are used as a surrogate model for the Bayesian optimisation scanning algorithm and for estimating the state of the 3D surface. A detailed explanation of GP regression can be found in Rasmussen and Williams (2006) and Murphy (2012). GP regression assumes a prior probability distribution over random functions f, which is defined by its mean function $m(x)$ and covariance function (also known as the kernel) $k(x, x')$:

$$f(x) \sim GP(m(x), k(x, x')) \tag{1}$$

where $m(x)$ and , $k(x, x')$ are:

$$m(x) = \mathbb{E}[\, f(x)] \tag{2}$$

$$k(x, x') = \mathbb{E}\Big[\big(f(x) - m(x)\big)\big(f(x') - m(x')\big)^T \Big] \tag{3}$$

The prior distribution of a discretised version $\hat{\boldsymbol{f}}$ of the random functions is a multivariate Gaussian distribution, denoted as:

$$\hat{\boldsymbol{f}} \sim N(\boldsymbol{\mu}, \boldsymbol{K}) \tag{4}$$

where $K_{i,j} = k(x_i, x_j)$ and $\boldsymbol{\mu} = (m(x_i), \dots, m(x_n))$. Suppose that some observations $\boldsymbol{y} = [y_1, \dots, y_N]^T$ have been obtained for some inputs $\boldsymbol{x} = [x_1, \dots, x_N]^T$. To predict the output $\hat{y}_*$ for a new input x_*, the GP regression model computes the posterior distribution using Bayes' rule, which can obtained analytically using the standard conditioning rules for the multivariate Gaussian distribution:

$$p(\, \hat{y}_* | x_*, \boldsymbol{x}, \boldsymbol{y}) = N(\mu_*, k_*) \tag{5}$$

where

$\mu_* = m(x_*) + \boldsymbol{k}_*{}^T \boldsymbol{K}^{-1}\big(\mathbf{y} - m(\boldsymbol{x})\big)$

$k_* = k(x_*, x_*) - \boldsymbol{k}_*{}^T \boldsymbol{K}^{-1} \boldsymbol{k}_*$

$\boldsymbol{k}_* = [k(x_1, x_*), \dots, k(x_N, x_*)]^T$

$\boldsymbol{K}$ = covariance matrix, $K_{ij} = k\big(x_i, x_j\big)$

In this study, two kernels were used. The first kernel is the Matérn kernel:

$$\kappa_{MA}(x - x') = \sigma^2 \frac{2^{1-\upsilon}}{\Gamma(\upsilon)} \left(\sqrt{2\upsilon}\frac{(x-x')}{\rho}\right)^{\upsilon} \mathcal{R}_{\upsilon}\left(\sqrt{2\upsilon}\frac{(x-x')}{\rho}\right) \tag{6}$$

which is used in the GP-based surrogate model for the Bayesian optimisation algorithm. The second kernel is the squared exponential kernel:

$$\kappa_{SE} = \theta_f^2 \exp\left(-\frac{1}{l^2}\|x - x'\|^2\right) \tag{7}$$

which is used in the GP regression model to predict the 3D surface. The squared exponential kernel assumes that the functions are smooth and is therefore well suited for modelling the 3D surface, whereas the Matérn kernel can model less smooth functions and may be better suited to modelling physical phenomena (Stein, 1999).The values of the kernel hyperparameters, such as σ_f^2 and l in Equation 7, are optimised by maximising the marginal log likelihood of the data, given the hyperparameters (Rasmussen and Williams, 2006).

The GP regression model in this study uses a zero-mean function because no prior assumptions are made about the shape of the surface. However, the predictions of the GP regression model are not heavily influenced by these prior assumptions as the GP model uses the observations to determine the posterior distribution of the regression function, which allows it to model arbitrarily complex shaped surfaces.

2.3 *Bayesian Optimisation*

Bayesian Optimisation (BO) is a popular machine learning (ML) method for finding the maximum of an unknown and expensive-to-evaluate objective function, $g(\boldsymbol{x})$, and is often expressed:

$$\boldsymbol{x}^* = \text{argmax}_x\big(g(\boldsymbol{x})\big). \quad (8)$$

BO has been used for many purposes including environmental monitoring (Marchant and Ramos, 2012), finding the optimum parameters for machine learning models (Wu et al., 2019) and physical devices such as lasers (Jalas et al., 2021), and controlling robots (Martinez-Cantin, 2017). BO is highly efficient (Shahriari et al., 2015) in terms of the number of function evaluations required to determine the nature of the objective function. One reason for its effectiveness is its ability to integrate prior knowledge in determining the optimal locations for sampling the objective function, while balancing the trade-off between exploration and exploitation. Exploration enables the algorithm to search areas with high uncertainty, while exploitation allows it to search areas where the objective function is expected to be high. By using a BO algorithm to control a 3D scanner, the goal is to reduce the number of measurements required to determine the nature of the soil plug surface, while also focusing on critical areas of the soil plug surface such as the most elevated areas. This reduces the time it takes to make a reliable prediction of the surface.

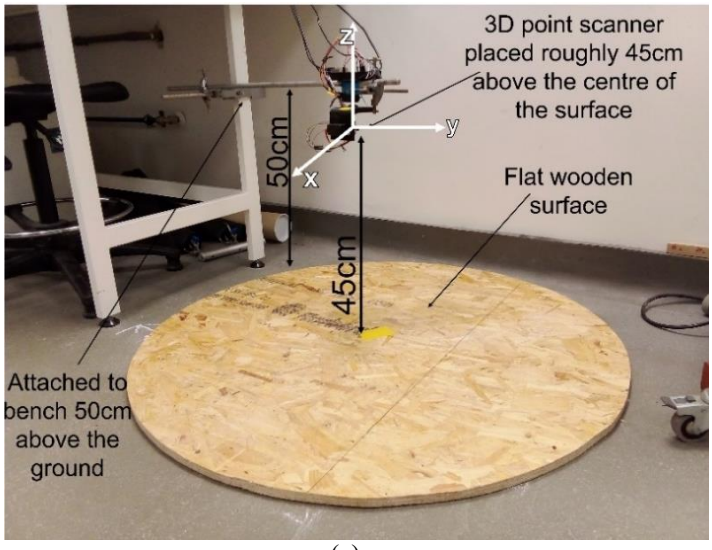

(a)

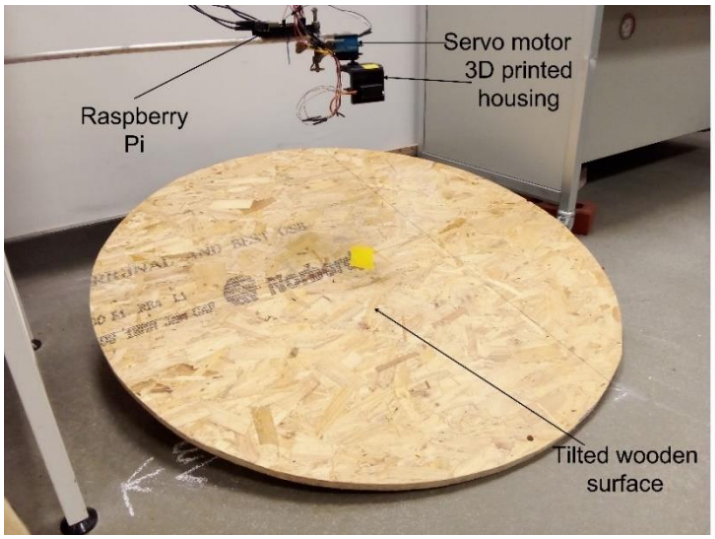

(b)

Figure 1: (a) Schematic diagram of experimental setup; (b) Photo of the experimental setup for the titled surface tests

BO involves a series of steps. First, a surrogate model is developed for the objective function. For the current study, a GP regression model is adopted for the surrogate model. An acquisition function is used to determine where to sample the objective function, based on the outputs of the surrogate model. The acquisition function identifies the location where the objective function is expected to be maximum, and this location is sampled next. The evaluation of the objective function at this location is then used to update the surrogate model, and the process is repeated.

The acquisition function used in this study is the "distance-based upper confidence bound" (DUCB) (Marchant and Ramos, 2012):

$$DUCB(x|x^-) \triangleq \mu(x) + \kappa \cdot \sigma(x) + \gamma \cdot d(x, x^-) \quad (9)$$

where $\mu(x)$ is the mean and $\sigma(x)$ is the variance of the surrogate model predictions, κ controls the exploration-exploitation trade-off, and $d(x, x^-)$ is the Euclidean distance between the last sampled location x^- and the candidate location x. The last term in Equation 4 represents a penalty term that aims to reduce the distance between sampling locations. This is particularly suitable for the 3D point scanning, as reducing the distance between each sampling location will reduce the time required to complete a scan.

2.4 *Experimental Procedures*

This paper evaluates the use of the BO algorithm for efficient 3D point scanning and GP regression for effective predictions of a 3D surface using a finite number of measurements. To this end, this paper presents the results of a preliminary experimental study that evaluates the performance of the BO scanning method and the GP regression method for the prediction of stationary surfaces in dry conditions. Although

this is not representative of the underwater environment for soil plug monitoring, the results serve as an initial feasibility assessment of the proposed methods before future tests are carried out underwater under more realistic conditions (e.g., dynamic moving soil surfaces). In this paper, the performance of the BO scanning method is also compared with that of the conventional scanning method.

A 3D point scanner was built, which consisted of a 2-axis rotating arm, made from 2 servo motors and a 3D printed housing, and a laser range finder (the Adafruit VL53L1X). A Raspberry Pi computer was used to control the servo motors and the laser range finder, in accordance with the sampling location suggestions from the BO and conventional algorithms. The 3D point scanner was positioned approximately 45cm above the ground, as shown in Figure 1a. The height at which the scanner was placed above the surface does not affect the measurements it takes or the ability of either scanning method. This distance was chosen to keep in scale with a caisson of length to diameter ratio of 0.5. Two sets of tests were performed: the first on a flat circular wooden surface of diameter 1m to mimic soil heave inside a caisson, and the second on a tilted circular wooden surface to mimic soil plug uplift. The tilted surface was created by propping up the same wooden surface used in the first set of tests at one end (see Figure 1b). Measurements of these surfaces were made to establish benchmarks of the true surfaces against which the predicted surfaces are compared. The following steps were performed for both flat and tilted surfaces. First, the conventional algorithm was run in its entirety to ensure that the construction of the 3D scanner was sound, and to assess whether there were any errors in the measurements taken by the laser range finder. Thereafter, both the BO and conventional scanning methods were run to collect 240 measurements. The measurements acquired by both scanning methods were each used as training data for a GP regression model to predict the state of the surface.

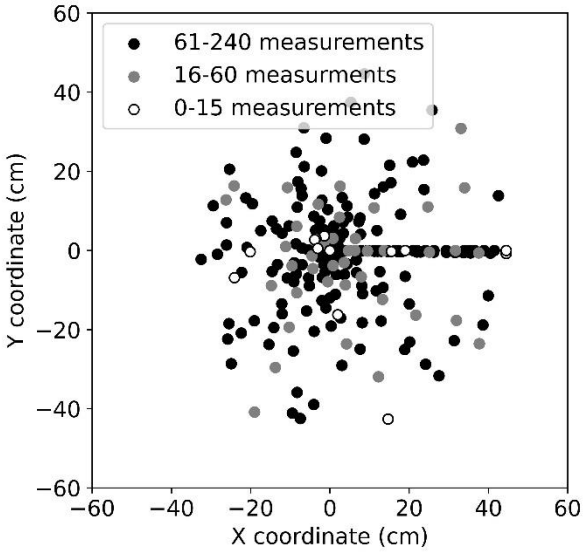

(a)

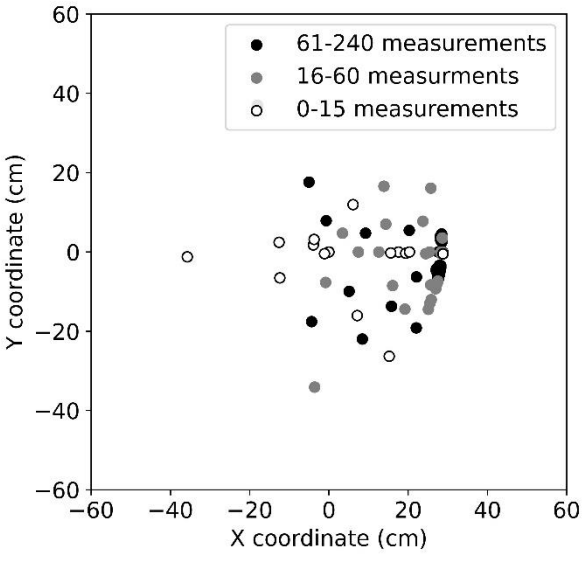

(b)

Figure 2: Distribution of measurement points collected by the BO scanning method, for (a) the flat surface and (b) the tilted surface

3 Results

The 3D point scanner measurements are presented in terms of Cartesian coordinates. The origin of the x, y, and z-axes is taken to be the location of the 3D point scanner, as shown in Figure 1a. Figure 2 shows the distribution of the measurements acquired by the BO scanning method for flat and tilted surfaces. Figure 2a shows that for the flat surface, the measurements are well distributed. The first 15 measurement points, shown as white markers, are very sparse; the next 45 measurement points, shown as grey markers, explore the surface to a greater extent and do not favour any particular area; the last 180 measurement points, shown as black markers, are well distributed across the surface too.

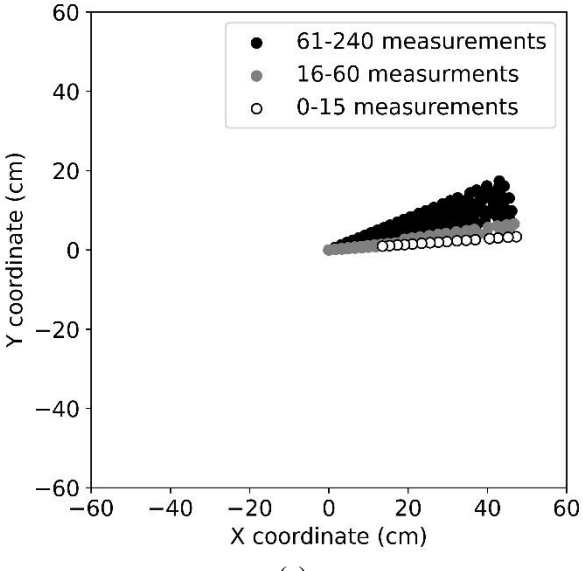

(a)

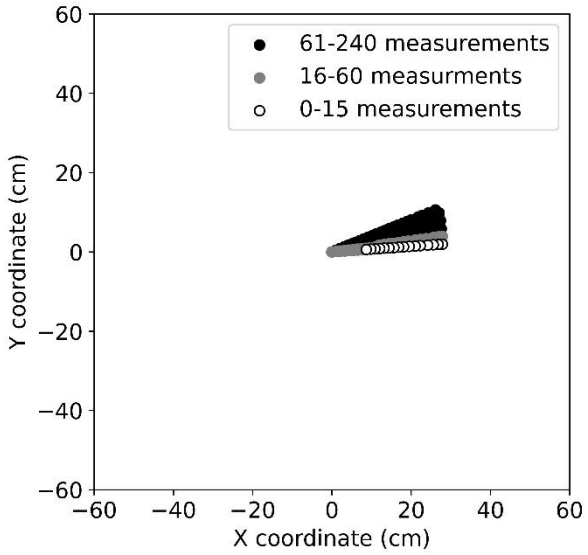

(b)

Figure 3: Distribution of measurement points collected by the conventional scanning method for (a) the flat surface and (b) the tilted surface

Figure 2b shows that the measurements for the tilted surface are much closer together than those for the flat surface. Initially, the whole surface is explored; the first 15 measurement points are well distributed across the surface but with some bias towards the raised side of the surface on the right-hand side. The following 45 and 180 measurement points were all taken on the raised side of the surface and are clustered around the highest part of the surface. Only four measurement points out of the last 225 were taken on the lower side of the surface, and these were in previously unexplored areas.

Similarly, Figure 3 shows the measurements acquired by the conventional scanning method for the flat and tilted surfaces. Evidently, there is little difference between Figures 3a and 3b. This is expected as the conventional algorithm does not adapt to the surface that it is scanning.

Figure 4 shows the surfaces predicted by the GP regression model trained on 60 and 240 measurements (represented by grey and black markers, respectively) obtained using the BO scanning method. These surfaces are represented by discrete point predictions for a large set of predefined locations across the surface. The true surface (represented by the white markers) is also included in Figure 4 for comparison. Areas closest to the scanner have z-coordinates less negative than those further from the scanner. As shown in Figure 4, the predicted flat and tilted surfaces agree well with the true surface. Nevertheless, Figure 4b shows that there are some errors between the true and predicted surfaces at the edges, where the predicted surfaces begin to level off instead of continuing the trend of the true surface.

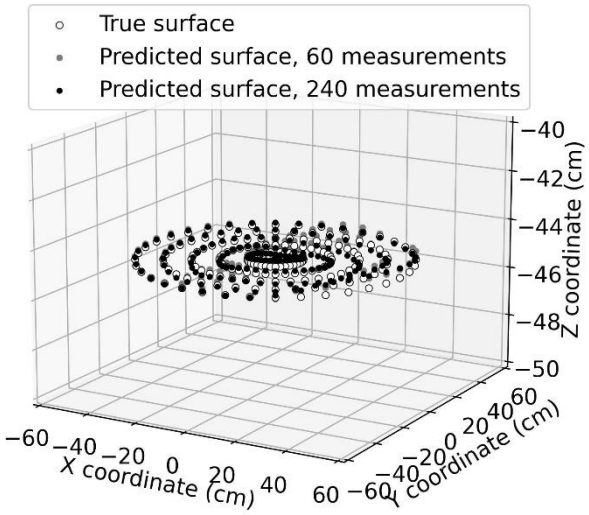

(a)

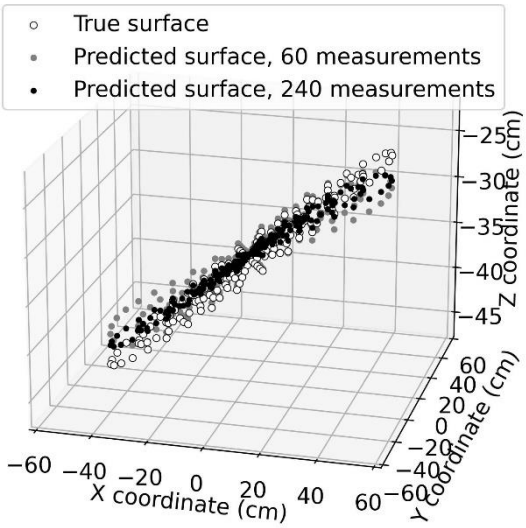

(b)

Figure 4: Comparison of the true surface (shown as white markers) against the surfaces predicted using 60 measurements (shown as grey markers) and 240 measurements (shown as black markers), acquired using the BO scanning method for (a) the flat surface and (b) the titled surface

Similarly, Figure 5 compares the surfaces predicted by the GP regression model trained on 60 and 240 measurements obtained by the conventional scanning method with the true surface. For the flat surface, the predicted surface agrees well with the true surface. However, for the titled surface, the error in the predictions is significant in areas where there are no measurements (i.e., the left side of the surface). On the right-hand side where the conventional scanning method acquired many measurements, there is better agreement between the predicted surface and the true surface.

To better quantify the errors between the predicted surfaces and the true surface, Figure 6 shows the relationship between the number of measurements and the root mean square (RMS) error between the predicted and true surfaces. The RMS error is calculated by summing up the difference in the two surfaces for

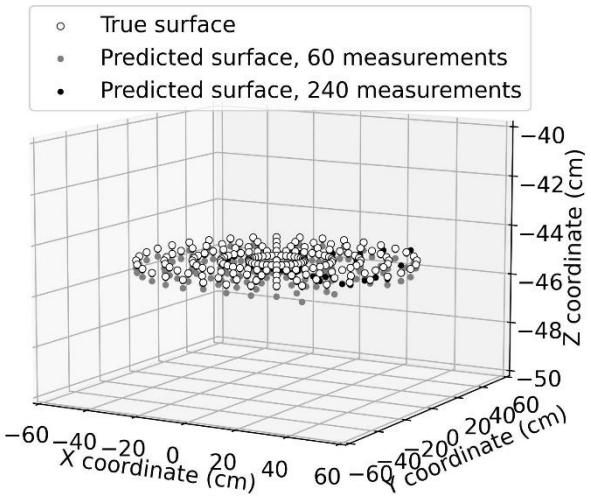

(a)

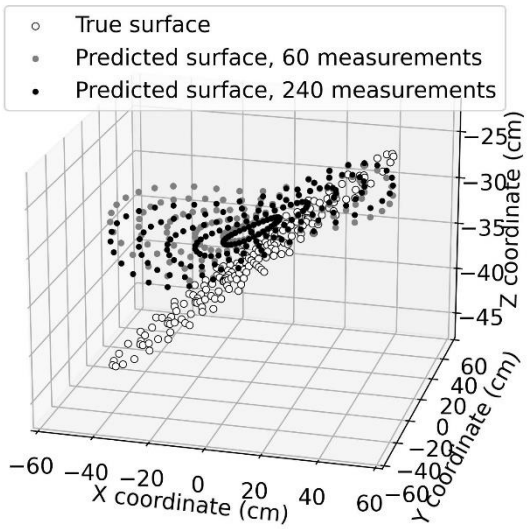

(b)

Figure 5: Comparison of the true surface (shown as white markers) with the surfaces predicted using 60 measurements (shown as grey markers) and 240 measurements (shown as black markers), acquired using the conventional scanning method for (a) the flat surface and (b) the titled surface

the predefined locations across the surfaces. It is evident from Figure 6 that the predicted surfaces by both scanning methods became more accurate as the number of measurements increased. For both flat and tilted surfaces, the predictions made using the measurements collected by the BO scanning method were more accurate than those collected by the conventional scanning method. Figure 6a shows that the flat surface predictions made using the measurements obtained by the BO scanning method are very accurate, even when using only 15 measurements points. Surface predictions made using the measurements obtained by the conventional method improved greatly as the number of measurements used increased to 60.

Figure 6b shows that the tilted surface predictions made using the measurements obtained by the BO scanning method reach maximum accuracy very quickly, after only 60 measurements. In contrast, the tilted surface predicted using the measurements obtained by the conventional scanning method improve only gradually with increasing number of measurements.

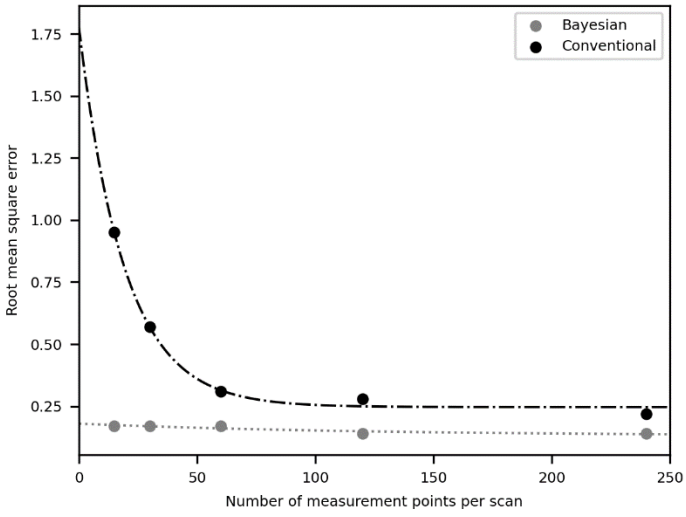

(a)

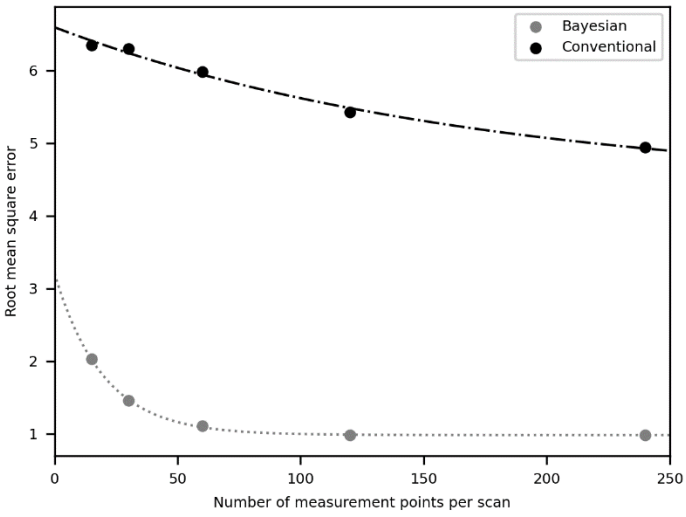

(b)

Figure 6: RMS errors between the true and predicted surfaces depending on how many measurements were used in the GP to make the prediction, for (a) the flat surface and (b) the tilted surface

4 Discussion

Figure 2 demonstrates that the BO scanning method can automatically adapt to different surfaces. The distribution of measurement points for flat and tilted surfaces is distinct, with measurements focused on the areas closest to the scanner for the tilted surface, as the BO algorithm aims to locate the maximum value within its search space. This outcome is suitable for monitoring soil plug hazards because the areas closest to the scanner pose the highest risk. By adapting to the surface, the BO scanning method produces predictions that are similar to the actual surface, as shown in Figure 4. Note that the κ parameter in Equation 9 of the BO scanning method can be adjusted to scan more of the unexplored areas of the soil plug

surface, instead of concentrating on the areas closest to the surface.

Figure 3 shows that the conventional algorithm did not adapt to the surface it was scanning, as there is minimal variation in the distribution of measurements for both the flat and tilted surfaces. Measurements acquired using the conventional scanning method were inadequate in capturing the features of the tilted surface, resulting in poor surface predictions that deviated significantly from the actual surface. This failure to adapt demonstrates the limitations of this method. This is evident in Figure 5b, where the predicted surfaces on the left side are significantly dissimilar to the true surface.

Although Figure 5a shows excellent agreement between predicted and true surfaces, it is crucial to note that this is because the GP model assumes a constant mean for areas with sparse data and not because the conventional method yielded informative measurements. To obtain accurate surface predictions using the conventional algorithm, a substantially larger number of measurements is necessary, as demonstrated in Figure 6.

Figure 6 indicates that the BO scanning method requires significantly fewer measurements (~60) to achieve maximum predictive accuracy compared to the conventional scanning method. The BO scanning method potentially provides a more efficient approach for real-time monitoring of soil plug hazards.

However, there are some limitations to this study. For instance, the experiments were conducted under conditions that do not accurately represent soil plug monitoring scenarios (e.g., dry instead of underwater conditions, laser range finder instead of sonar device, stationary instead of moving surface, wooden surface instead of soil surface). Additionally, in more realistic conditions, measurements may feature higher levels of noise, although it is noted that the GP regression model is a probabilistic model capable of handling noisy measurements. Furthermore, these tests did not include an irregular surface with local minima and maxima that would more closely mimic the ocean floor. In this case, the Bayesian scanning method may use more resources searching some local maxima, but it will not be stuck there as it will not neglect to scan unexplored areas of the surface. Thus, it may take more measurements for the irregular surface estimations to reach the same level of accuracy as the regular surfaces tested.

Future research will focus on addressing the limitations presented in the discussion section. The device will be tested in more realistic conditions, involving a moving surface underwater in clear and turbid conditions. Several other surface orientations and trajectories will also be tested. For example, an irregular surface featuring local maxima and minima will be tested. The laser range finder will be replaced with either a single beam echosounder or underwater laser range finder, and all electrical components will be made waterproof. The method will be adapted to the more complex spatio-temporal problem of monitoring the state of a dynamically moving surface. It will be tested with measurements that have been corrupted with artificial noise, in order to assess its ability to cope with noisy data. In addition, a method for choosing initial measurements will be developed. One such method is the 'Latin hyper cube design' as discussed in Nyikosa (2018).

5 Conclusion

This study proposes a new AI-driven 3D point scanner, which is controlled by an adaptive Bayesian Optimisation algorithm. The results indicate that the proposed scanner can accurately estimate a flat and tilted surface using much fewer measurements than the conventional method. Thus, the proposed scanner presents a potentially more effective method for real-time monitoring of soil plug hazards during suction caisson installation.

6 References

Aas, P.M., Saue, M. and Aarsnes, J. (2009). Design predictions and measurements during installation of suction anchors with and without water-flow system to help installation through layered soil profiles. In Offshore Technology Conference 9.

Andersen, K.H. and Jostad, H.P. (2002). Shear strength along outside wall of suction anchors in clay after installation, Proceedings of the12th ISOPE Conference, Kyashu, Japan, paper No. 2002-PCW-02.

Byrne, B., Houlsby, G., Martin, C. and Fish, P. (2002). Suction caisson foundations for offshore wind turbines. Wind Engineering, 26(3): 145-155.

Cain, C. and Leonessa, A. (2012). Laser based rangefinder for underwater applications. In 2012 American control conference (acc), 6190-6195pp.

He, B., Yang, S. and Sturm, H. (2022). Case studies on suction caisson foundations in offshore wind farms in China. International Journal of Geotechnical Engineering, 16(8): 917-933.

Jalas, S., Kirchen, M., Messner, P., Winkler, P., Hübner, L., Dirkwinkel, J., Schnepp, M., Lehe, R. and Maier, A.R. (2021). Bayesian optimization of a laser-plasma accelerator. Physical review letters, 126(10): 104801.

Marchant, R. and Ramos, F. (2012). Bayesian optimisation for intelligent environmental monitoring. In 2012 IEEE/RSJ international conference on intelligent robots and systems, 2242-2249pp.

Martinez-Cantin, R. (2017). Bayesian optimization with adaptive kernels for robot control. In 2017 IEEE international conference on robotics and automation (ICRA) 3350-3356pp

Murphy, K.P. , Machine learning: a probabilistic perspective, The MIT press (2012), ISBN 978-0-262-01802-9, 515 – 542pp

Nyikosa, F.M. (2018). Adaptive Bayesian optimization for dynamic problems. PhD thesis, University of Oxford.

OWA (2019). Suction Installed Caisson Foundations for Offshore Wind: Design Guidelines. Carbon Trust.

Ragni, R., Bienen, B., O'Loughlin, C.D., Stanier, S.A., Cassidy, M.J. and Morgan, N. (2020). Observations of the effects of a clay layer on suction bucket installation in sand. Journal of Geotechnical and Geoenvironmental Engineering, 146(5): 04020020.

Rasmussen, C.E. and Williams, C.K. . Gaussian processes for machine learning Vol. 1, p. 159. The MIT press (2006), ISBN 026218253X, 7-30pp

Shahriari, B., Swersky, K., Wang, Z., Adams, R.P. and De Freitas, N. (2015). Taking the human out of the loop: A review of Bayesian optimization. Proceedings of the IEEE, 104(1): 148-175.

Sparrevik, P., Strout, J., & Meyer, V. (2015). Novel monitoring solutions solving geotechnical problems and offshore installation challenges. Frontiers in Offshore Geotechnics III, 319-324pp.

Stein, M.L. . Interpolation of spatial data: some theory for kriging. Springer Science & Business Media (1999), ISBN 978-1-4612-1494-6, 249pp

Suryasentana, S. K., and Sheil, B. B. (2023). Demystifying the connections between Gaussian Process regression and kriging theories. In 9th International Conference on Offshore Site Investigation and Geotechnics, London, UK.

Wu, J., Chen, X.Y., Zhang, H., Xiong, L.D., Lei, H. and Deng, S.H. (2019). Hyperparameter optimization for machine learning models based on Bayesian optimization. Journal of Electronic Science and Technology, 17(1): 26-40.

Zhang, Y., Guo, Y., Wei, H., Lou, L., Song, H., Yang, P. and Liu, C. (2017). Influence of water on underwater distance measurement by a laser range finder. In OCEANS 2017-Aberdeen, 1-5pp